ELSEVIER

Journal of Hydrology 269 (2002) 194–207

Journal of Hydrology

www.elsevier.com/locate/jhydrol

Mapping spatial variation in surface soil water content: comparison of ground-penetrating radar and time domain reflectometry

J.A. Huisman*, J.J.J.C. Snepvangers, W. Bouten, G.B.M. Heuvelink

Center for Geo-ecological Research (ICG), Institute for Biodiversity and Ecosystem Dynamics (IBED), Physical Geography, Universiteit van Amsterdam, Nieuwe Achtergracht 166, 1018 WV Amsterdam, The Netherlands

Received 30 August 2001; revised 22 July 2002; accepted 31 July 2002

Abstract

Mapping soil water content (SWC) is a difficult but important task in many fields, such as hydrology, agronomy and soil science. Ground-penetrating radar (GPR) is a valuable technique to measure surface SWC at an intermediate scale in between the scales of time domain reflectometry (TDR) and remotely sensed data. To measure SWC with GPR, the surface soil permittivity was determined with the ground wave velocity. The first aim of this study was to evaluate the potential of GPR to measure spatial SWC variation. The second aim was to compare GPR and TDR with respect to the type of spatial SWC structures that can be measured by these methods. A spatial structure in SWC was created by heterogeneous irrigation with sprinklers of various intensities. Then spatial SWC variation was measured with both GPR and TDR. The experiment showed that GPR is well able to measure spatial SWC variation as expressed by the variogram. The larger measurement volume of GPR filtered out small-scale spatial variation (<1.5 m) and the large number of easily acquired GPR measurements resulted in well-defined and smooth experimental variograms. A comparison of interpolated SWC maps before and after irrigation showed that GPR is better suited than TDR for mapping large-scale features (>5 m) in SWC. Especially the boundaries between areas with different SWC were better resolved in case of GPR because of the large number of GPR measurements obtained with the same measurement effort. Small-scale features (<5 m) were not mapped adequately by either GPR or TDR. However, the chance of detecting small-scale features in SWC mapping at the field scale is higher for GPR, simply because of the higher sampling density.

Keywords: Soil moisture; Ground-penetrating radar; Time domain reflectometry; Spatial variation

1. Introduction

The spatial variation of surface soil water content (SWC) is an important variable at a wide range of scales. At a large or continental scale, SWC variation is important for the parameterization of coupled land-atmosphere models and weather forecast models. For example, Wood (1997) showed that grid-scale estimates of transpiration are sensitive to the presence or absence of subgrid-scale variation in SWC. At an intermediate or catchment scale, SWC variation influences the partitioning of precipitation into infiltration and runoff and, therefore, exerts a strong control on discharge predictions. This was illustrated by Merz and Bardossy (1998), Yu (2000) and Western et al. (2001), who showed that there can

* Corresponding author. Tel.: +31-20-525-7450; fax: +31-20-525-7431.
E-mail address: s.huisman@science.uva.nl (J.A. Huisman).

0022-1694/02/$ - see front matter © 2002 Elsevier Science B.V. All rights reserved.
PII: S0022-1694(02)00239-1

be substantial differences between runoff simulations with and without spatial variation (and connectivity) in SWC. At an even smaller scale, SWC variation caused by preferential flow can lead to accelerated breakthrough of solutes, such as some pesticides and heavy metals, and can, therefore, affect groundwater quality (Ritsema and Dekker, 1998).

Available techniques to assess spatial variation of SWC, hereafter referred to as mapping, are either suited to measure small-scale (m^2) or large-scale (km^2) variations. Time domain reflectometry (TDR, Topp et al., 1980) and capacitance measurements (Paltineanu and Starr, 1997), have a small measurement volume of 0.01–1 dm^3. This makes them especially useful to measure small-scale processes up to several m^2, such as fingered flow (Nissen et al., 1999) and soil water dynamics due to spatial variation in throughfall (Bouten et al., 1992). However, SWC mapping at a larger scale (up to several ha) with these techniques requires a large number of measurements in order to provide an adequate sampling density. This is not easily achieved with these small-scale measurement techniques because they are invasive and therefore labor-intensive.

Remote sensing with either passive microwave radiometry or active radar instruments is the only promising technique for mapping SWC of large regions (Jackson et al., 1996; Famiglietti et al., 1999). The passive instruments have low spatial resolution (large footprint) and can be either airborne with footprints of hundreds of meters or satellite-borne with footprints of tens of km. Active radar instruments have small footprints ranging from 10 to 100 m from air or space. Most often, the SWC variation within the remote sensing footprint will be large due to topography, microclimate, tillage, water uptake by trees and crops (Famiglietti et al., 1999; Mohanty et al., 2000; Hupet and Vanclooster, 2002). The presence of non-linear relationships between SWC and hydrological processes such as evapotranspiration and infiltration requires knowledge of the spatial variation of SWC within the remote sensing footprint to optimally utilize remotely sensed data.

Currently there is a scale gap between commonly used field (point) measurements and large-scale remote sensing measurements. One possibility to bridge this gap in order to obtain SWC variation at an intermediate scale is to use small-scale measurement techniques within the frameworks of spatial aggregation and geostatistics (Heuvelink, 1998; Western and Blöschl, 1999). Another possibility is to develop SWC measurement techniques that measure directly at the scale of interest. Ground-penetrating radar (GPR) is a promising technique for mapping surface SWC at the intermediate (ha) scale. GPR has a measurement volume ranging from 0.05 to 20 m^3 depending on the antenna frequency and radar configuration used to measure SWC (Du and Rummel, 1994; Chanzy et al., 1996; van Overmeeren et al., 1997; Weiler et al., 1998). In this paper, 225 MHz antennas with a fixed antenna separation of 1.54 m were used to determine the ground wave velocity. The ground wave is a direct wave traveling from source to receiving antenna through the topsoil and the velocity of this wave is strongly related to the SWC of the upper centimeters of the soil (Du and Rummel, 1994; Sperl, 1999; Huisman et al., 2001). The measurement volume with this type of GPR measurement is 0.05–0.07 m^3.

The aim of this study is twofold. The first aim is to evaluate the potential of GPR to map SWC of an area of 3600 m^2. This relatively small field size was chosen to allow a practical comparison of GPR and TDR measurements. The second aim is to compare the types of spatial SWC structures that can be measured by GPR and TDR. This is relevant since GPR and TDR have different measurement volumes and could, therefore, measure different types of spatial SWC structures. We did an irrigation experiment in which various spatial structures were created by using sprinklers of different size and sprinkling intensity. Before and after irrigation, 12 GPR transects of 60 m consisting of 121 measurements each and 216 TDR measurements were collected. This sampling density represents an equal measurement effort for GPR and TDR. Interpolated maps of SWC were calculated by kriging and compared to evaluate the usefulness of GPR for mapping SWC and to see whether different types of spatial SWC structures created by irrigation could be measured by GPR and TDR.

2. Theory of ground-penetrating radar

The GPR technique is similar in principle to reflection seismics and sonar techniques. The radar produces a high-frequency electromagnetic wave

(10–1000 MHz), which is transmitted into the soil by a source antenna placed on the earth surface. The propagation velocity of the radar waves in the soil mainly depends on the soil dielectric permittivity, which in turn is strongly related to SWC (Topp et al., 1980). Any subsurface contrast in dielectric properties will reflect part of the wave energy back to the surface. The reflected wave is detected by the receiving antenna as a function of time (Davis and Annan, 1989). Fig. 1 shows possible propagation paths of the radar waves in a two-layer soil. The propagation velocity of these waves can be used to estimate the permittivity of the topsoil, ε_1 (and therewith SWC). For example, van Overmeeren et al. (1997) and Weiler et al. (1998) used the velocity of waves reflected from a soil horizon (interface ε_1 to ε_2 in Fig. 1) to determine SWC. Unfortunately, the velocity of reflected waves cannot be determined from a single offset radar measurement without knowledge of the depth to the reflecting soil horizon, which can only be determined by intensive drilling in most cases. Du and Rummel (1994) suggested that the ground wave is the most promising wave for SWC mapping if there is no well-defined reflection from a soil horizon. The ground wave is the wave traveling directly from source to receiving antenna through the top of the soil and therefore it is the only wave of which the propagation distance can be known a priori (also see Du (1996) and Sperl (1999)). The theory of the ground wave is not completely understood but approximate solutions of electrical field distributions around a source antenna (a Horizontal Electrical Dipole) placed at the soil surface do indicate that the ground wave decays faster ($1/r^2$) with increasing propagation distance r than a reflected wave which decays as $1/r$ (Annan, 1973; Brekhovskikh, 1960; van der Kruk, 2001). This inverse square decay and the influence of soil electrical conductivity limit the range of antenna separations at which the ground wave can be observed to about 5 m in sandy soils and to 1 m or less in heavily textured soils for 225 MHz antennas.

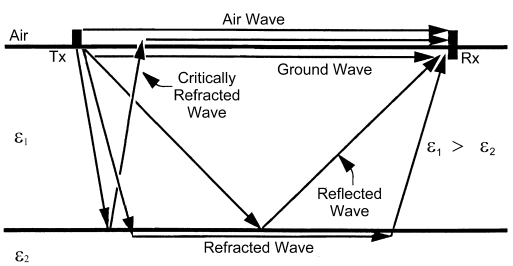

Fig. 1. (After Sperl, 1999): Propagation paths of electromagnetic waves in a soil with two layers of contrasting dielectric permittivity (ε_1 and ε_2).

The ground wave can be identified in a wide angle reflection and refraction (WARR) measurement (left part of Fig. 2). WARR acquisition consists of increasing the distance between the antennas stepwise while one antenna remains at a fixed position. The direct path of the ground wave between source and receiver through the top of the soil results in a linear relationship between arrival time and antenna separation. This allows identification of the ground wave and easy determination of the ground wave velocity (and dielectric permittivity) from the tangent line as indicated with V_{WARR} in Fig. 2. However, the acquisition time of a WARR measurement is long and the required changes in antenna separation make this procedure impractical for SWC mapping.

The ground wave velocity can also be determined from a single radar measurement with a known antenna separation (single trace analysis (STA)) if the ground wave has been identified in a WARR measurement. In this case, it is possible to place the antennas on sleds, thus providing the mobility to quickly map large areas. The right part of Fig. 2, marked with STA, shows a schematic GPR transect obtained by moving the sender and receiver over an abrupt change in relative permittivity from 10 to 15 at 4 m with a fixed antenna separation of 2.5 m. In case of the STA, the ground wave velocity cannot be obtained from the change in arrival time with increasing antenna separation as with the WARR measurement. Therefore, the ground wave velocity, v (ms^{-1}), and the STA refractive index (n_{STA}; square root of permittivity ε) are calculated from a single trace at a known antenna separation x (m) with

$$n_{STA} = cv^{-1} = c\left(\frac{x}{(t_{GW} - t_{AW}) + c^{-1}x}\right)^{-1} = \frac{c(t_{GW} - t_{AW}) + x}{x} \quad (1)$$

where c is the electromagnetic wave velocity in air (3×10^8 ms^{-1}) and t_{GW} (s) and t_{AW} (s) are the arrival times of the ground wave and the air wave. Time picks indicating the arrival time of the air

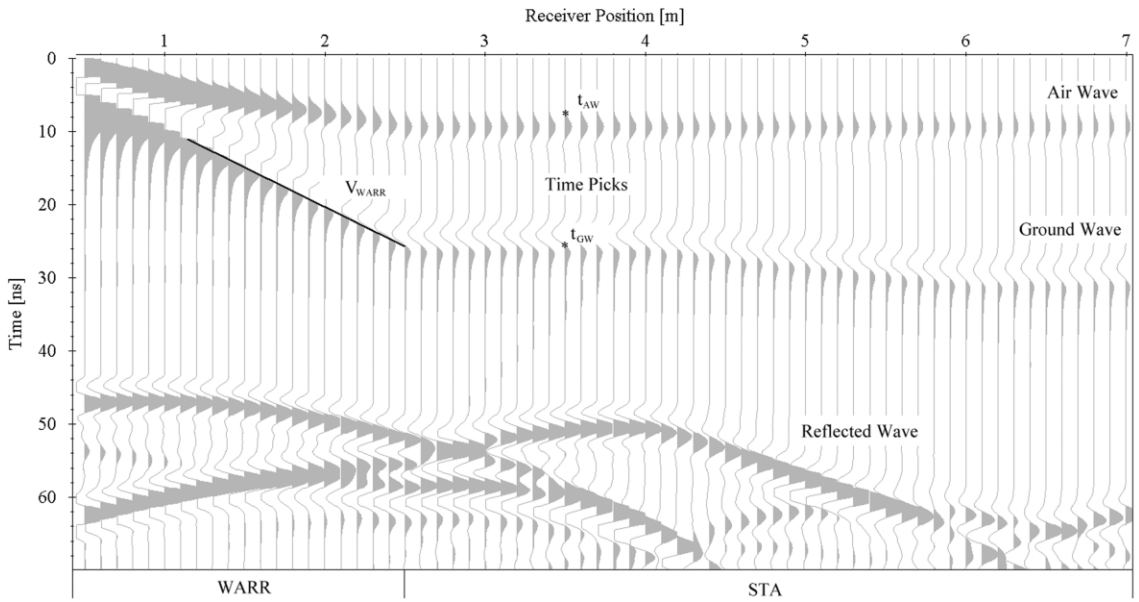

Fig. 2. Schematic WARR-measurement (left side) and a STA transect (right side) measured over a change in permittivity positioned at 4 m (relative permittivity of 10 at left side and 15 on right side). V_{WARR} indicates the tangent line used to calculate the ground wave velocity from WARR measurements. The time picks t_{GW} and t_{AW} are the arrival time of the ground and air wave, respectively.

wave and the ground wave are marked with stars in Fig. 2 for one trace. The arrival time of the ground wave starts increasing at 4 m because the receiver has passed the abrupt change in soil permittivity. The ground wave arrival time keeps increasing until the sender has passed the abrupt change in soil permittivity, i.e. a receiver position of 6.5 m. Clearly, abrupt boundaries are smoothed by GPR due to the averaging along the propagation path between source and receiving antenna.

The measurement volume of SWC measurements with the ground wave is determined by the antenna separation, the width of the antenna and the influence depth of the ground wave. Unfortunately, the depth of influence of the ground wave is not well defined. Du (1996) suggested that the influence depth is approximately half of the wavelength ($\lambda = c/(f\varepsilon^{1/2})$) which would, for example, mean that the depth of influence varied from 0.50 m ($\varepsilon = 4.0$) to 0.22 m ($\varepsilon = 20.0$) for the 225 MHz antennas. Sperl (1999) reported that the depth of influence was indeed a function of wavelength, but from a modeling exercise he concluded that the influence depth is $\approx 0.145\lambda^{1/2}$, which would suggest that the influence depth ranges from 0.15 m ($\varepsilon = 4.0$) to 0.10 m ($\varepsilon = 20.0$) for the 225 MHz antennas. The results of Sperl (1999) do not contradict those of Huisman et al. (2001), who concluded that SWC measurements made with the ground wave of GPR are similar to SWC measurements with 0.10 m long TDR probes for both the 225 and 450 MHz antennas.

3. Materials and methods

3.1. Irrigation experiment

A heterogeneous SWC pattern was created by irrigation with four types of sprinklers differing in radius and sprinkling intensity. The idea behind the design of the irrigation experiment was to introduce different types of spatial structures to find out what type of patterns can be measured by GPR and TDR. The measurement site was 60×60 m^2 and located within a pasture in Molenschot, the Netherlands (51°35′N and 4°52′E). The soil was classified as a Plaggept according to the Soil Taxonomy by USDA (1975). The textural class of the topsoil was sandy loam as determined by grain-size analysis of 25 samples (average weight percentage of dry mineral

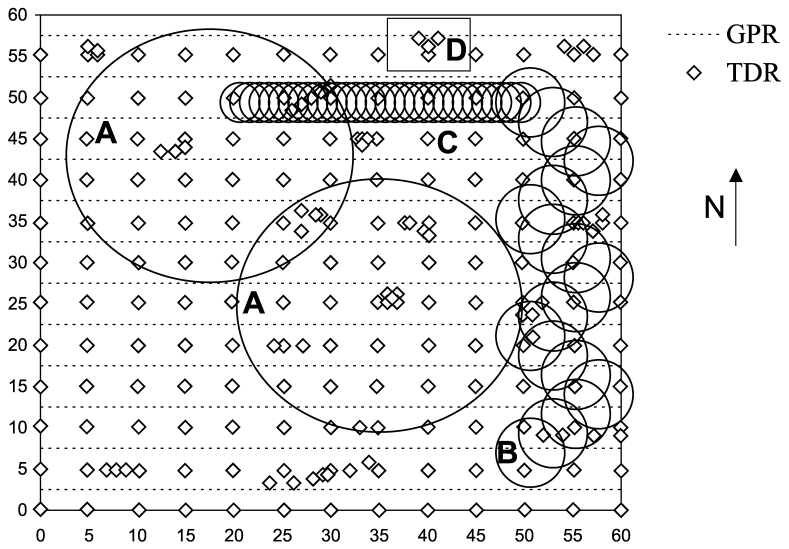

Fig. 3. Schematic representation of the different types of SWC structures created by irrigation with four different kind of sprinklers (marked A–D).

matter was 67% sand, 30% silt and 3% clay). Beneath the sandy loam there was a less permeable clay layer at 0.9–1.0 m depth, which periodically caused water stagnation as evidenced by gley mottles within the loamy sand from 0.75 to 0.90 m. Ditches bound the field on the north and east side.

The location of the sprinklers is shown schematically in Fig. 3. Details of the four types of sprinklers (A–D) are given in Table 1. Two large impact sprinklers (type A) with a prescribed radius of 10–15 m located at (17.5,42.5) and (35,25) created two large areas with increased SWC. A straight line of 31 micro-sprinklers (type C) with a prescribed radius of ~2 m running from (20,50) to (50,50) and a zigzag sprinkler line of 19 micro-sprinklers (type B) with a prescribed radius of ~3.5 m created two narrow zones of high SWC. Finally, a lawn oscillator sprinkler located at (40,55) introduced a small square area of higher SWC. The radius of each type of sprinkler as a function of direction was determined with collecting cups with an average diameter of 0.099 m. This information was then used to generate a map indicating the area that was irrigated by the sprinklers, which was very similar to Fig. 3. The irrigation experiment was done on 17 August 2000. The irrigation started at 6:00 AM and lasted to 7:30 AM for the high intensity sprinklers (types B, C and D) and to 10:00 AM for the type A sprinklers. During irrigation, a meteorological station located at 2 m height in the SW corner of the field recorded that the average wind direction was SW, the average wind speed was 2.2 ms^{-1} and the average temperature was 17 °C. In total, 33 m^3 of water was applied. GPR and TDR measurements were carried out before irrigation (16 August, 12:30 PM) and after irrigation (17 August, 11:45 AM). Between both measurement rounds, it rained another 2 mm overnight.

3.2. Ground-penetrating radar

We used a pulseEKKO™ 1000 GPR system with a 200 V transmitter (Sensors and Software, Mississauga, Ont., Canada) and broadband antennas with a center frequency of 225 MHz (in air) and a frequency bandwidth of 225 MHz (Davis and Annan, 1989).

Table 1
Description of four types of sprinklers used in the irrigation experiment

Sprinkler	Number	Time (h)	Area (m^2)	Amount (mm)	*M*
A	2	4	1240	14	35
B	19	1.75	450	20	24
C	30	1.75	114	50	18
D	1	1.75	75	17	18

Radius and amount of water for each type of sprinkler was determined with *M* cups.

The radar data were collected with the acquisition software supplied by the manufacturer. We measured 12 transects of 60 m (Fig. 3) with a time window of 60 ns, a sampling rate of 60 ps and 16 stacks per trace. The transect measurements were made by placing the antennas on sleds with an antenna separation of 1.54 m, which means that the measurement volume of the GPR measurement was 0.05–0.07 m^3, depending on the water content of the soil. The radar was triggered each 0.5 m with an odometer (Fig. 4), which resulted in 121 measurements per transect. The southernmost transect was only 45 m due to the presence of the meteorological station in the SW corner of the field. Therefore, the number of GPR measurements was 1422. The two sleds were connected by rigid poles and the antennas were strapped to the sleds to ensure a fixed antenna separation of 1.54 m. No metallic components were used in the construction of the sleds in order to minimize electromagnetic interference of the radar by the sleds. The sleds and radar equipment were pulled with a three-wheeled electric scooter at a speed of approximately 0.7 km h^{-1}. Each GPR transect was acquired and processed separately. REFLEX (Sandmeier Scientific Software, Karlsruhe, Germany) was used for standard GPR data processing, including a 'dewow'-filter to remove low-frequency induction effects of the radar equipment and a down-trace averaging filter to remove noise. The GPR refractive index, n_{STA}, was determined with Eq. (1). The arrival times of the air and ground wave were obtained by semi-automated time picking in REFLEX. In case of the air wave, the average arrival time per transect was used. This was necessary because the air wave was disturbed and therefore not equally recognizable in each trace due to (1) equipment present in the vicinity of the antennas and (2) the reduced and variable contact (coupling) between antennas and soil when the antennas are placed on sleds and pulled. The acquisition time of the GPR measurements was approximately 75 min and the processing time was 45 min.

3.3. Time domain reflectometry

We collected 156 TDR measurements on a 5×5 m^2 grid and 60 nested TDR measurements to estimate short distance variation. This makes a total of 216 TDR measurements marked with diamonds in Fig. 3. The position of each sampling location was determined with a theodolite. A Tektronix 1502 cable tester (Beaverton, OR, USA) was used with a 0.10 m long three-wire probe described by Heimovaara (1993). All TDR measurements were carried out manually by vertically inserting the TDR probe in the topsoil. The measurement volume of TDR depends on

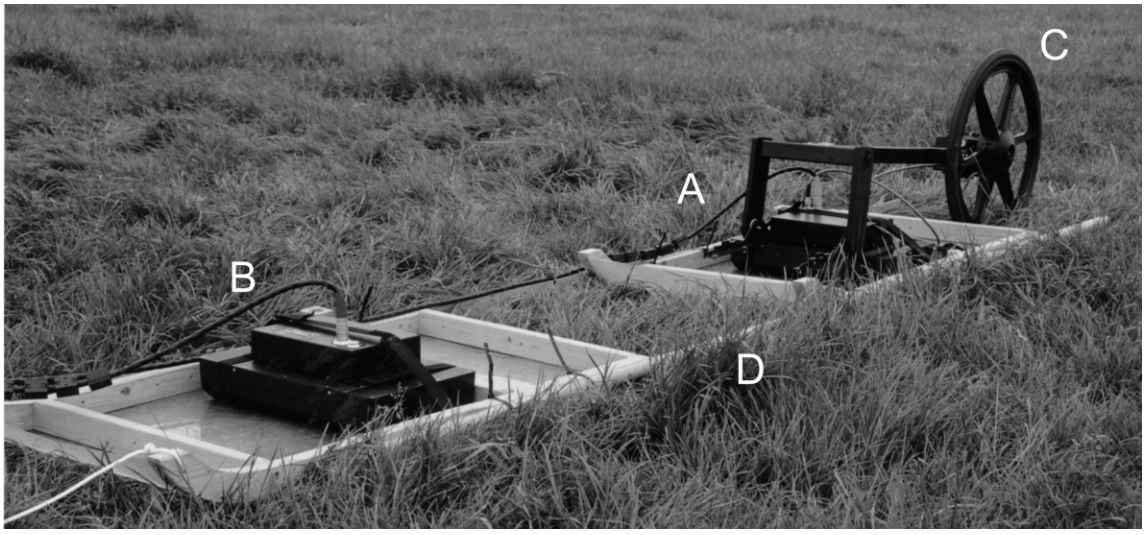

Fig. 4. Equipment used to measure GPR transects. (A) Source antenna, (B) receiving antenna, (C) odometer used to trigger radar equipment every 0.5 m and (D) rigid poles to ensure a fixed antenna separation of 1.54 m.

the type of probe, and is mainly determined by the length, number, thickness and separation of the wires. In case of our 0.10 m long three-wire probes, the measurement volume is approximately equal to 3×10^{-5} m^3 (Ferré et al., 1998). The TDR refractive index of the soil was calculated according to

$$n_{\mathrm{TDR}} = \frac{c\Delta t_{\mathrm{s}}}{2L} \tag{2}$$

where Δt_{s} (s) is the travel time of the electromagnetic signal in the soil obtained with the travel time analysis presented in Heimovaara and Bouten (1990). The acquisition time for the TDR measurements was approximately 90 min and the travel time analysis took 15 min.

3.4. SWC calibration

A site-specific calibration equation between refractive index and SWC was determined with the method proposed by Herkelrath et al. (1991). We used 14 soil samples taken from the topsoil in 0.10 m high and 0.05 m diameter stainless steel rings. After wetting the samples, the refractive index (n_{a}) as a function of SWC (θ) was determined by drying the samples on a balance, while simultaneously performing TDR measurements with 0.10 m sensors. This procedure resulted in the following calibration equation

$$\theta = 0.1116 n_{\mathrm{a}} - 0.1543, \qquad R^2 = 0.9865 \tag{3}$$

which is based on 192 TDR measurements from 14 samples in the water content range of 0.1–0.4 m^3 m^{-3}. Huisman et al. (2001) showed that there was little difference between the calibration equation predicting θ from n_{STA} or n_{WARR} and the one predicting θ from n_{TDR}. Therefore, Eq. (3) was used to convert GPR and TDR measurement to SWC.

3.5. Comparison of GPR and TDR

GPR and TDR measurements were compared in two ways. First, the spatial SWC variation measured with GPR and TDR was compared with an approximation of the spatial variation of the irrigation pattern. Second, interpolated maps of SWC based on GPR and TDR measurements were compared to see which kinds of spatial structures in SWC were measured by GPR and TDR.

The semivariance between measurements at locations x and $x + h$ is defined as

$$\gamma(h) = \tfrac{1}{2} E[\{z(x) - z(x+h)\}^2] \tag{4}$$

where E signifies expectation and h is the distance separating x and $x + h$. The function relating semivariance to h, is the variogram. Spatial correlation manifests itself in the variogram by a monotonic increase from the origin with increasing h. The variogram as expressed in Eq. (4) must be estimated from the data and this is done by fitting a variogram model to the experimental variogram, which is computed from the data according to

$$\hat{\gamma}(h) = \frac{1}{2N(h)} \sum_{i=1}^{N(h)} [z(x_i) - z(x_i + h)]^2 \tag{5}$$

where $N(h)$ is the number of pairs of observations separated by a distance h and $z(x_i)$ denotes an observation at location x_i (see Goovaerts, 1997 or Webster and Oliver, 2001). Different types of variogram models can be fitted to the experimental variogram. In this study, the spherical model is used

$$\gamma(h) = \begin{cases} 0 & \text{for } h = 0 \\ c_0 + c\left[1.5\dfrac{h}{a} - 0.5\left(\dfrac{h}{a}\right)^3\right] & \text{for } 0 < h \le a \\ c_0 + c & \text{for } h > a \end{cases} \tag{6}$$

The nugget variance c_0 (m^3 m^{-3})^2 represents small-scale variation and measurement error. The range a (m) describes the correlation length. In the spherical model, the semivariance between two measurements becomes constant at distances larger than the range where the sill variance $c_0 + c$ (m^3 m^{-3})^2 is reached.

The parameters of the spherical model, except for the TDR nugget variance, were fitted by a least-squares procedure, after detrending the data with a second-order polynomial trend plane in the x–y coordinates. In order to not disturb the comparison between GPR and TDR, the GPR and the TDR measurements were detrended with the same trend plane calculated from the GPR measurements. The TDR nugget variance was determined by taking extra TDR measurements within 1 m distance and estimating the nugget of the 'small-scale' variogram calculated from these extra TDR measurements.

The comparison between GPR and TDR variograms is more meaningful after compensation for the difference in measurement volume (i.e. the 'support' in geostatistical terms). This can be done by regularization of the point variable $z(y)$, in our case the TDR measurements, over the volume w, in our case the support of GPR

$$z_w(x) = \frac{1}{w}\int_w z(y)\mathrm{d}y \tag{7}$$

The mean value $z_w(x)$ is said to be the regularization of the point variable $z(y)$ over the volume w. The problem now is to derive the regularized variogram

$$\gamma_w(h) = \tfrac{1}{2}E[\{z_w(x) - z_w(x+h)\}^2] \tag{8}$$

from the point variogram $\gamma(h)$. This was done numerically according to the procedures described in Journel and Huijbregts (1978, pp. 77–94).

To compare SWC variograms for GPR and TDR with the variogram of the irrigation pattern, the reconstructed irrigation map was used to calculate indicator variograms. We assigned 1's to irrigated areas and 0's to non-irrigated areas and used Eqs. (4) and (5) to calculate variograms. These indicator variograms are a first approximation of the SWC pattern created by irrigation because the large amount of irrigation resulted in saturated SWCs (1's) where irrigation was applied and drier conditions where no irrigation was applied (0's). A second-order polynomial trend plane in the $x-y$ coordinates was subtracted to obtain stationary variograms, which implies that the resulting variograms are not indicator variograms in the true sense.

GPR and TDR were also compared in terms of interpolated maps of SWC before and after irrigation. Interpolations were made on a $1 \times 1\ \mathrm{m}^2$ grid with universal kriging, which allows the inclusion of trends in the interpolation. To compensate for the difference in support between GPR and TDR, block kriging was used for the TDR measurements. In block kriging, a block support w, the GPR support (1.54 m × 0.30 m), is used to estimate the mean SWC for blocks. The variogram modeling and the geostatistical interpolation were done with GSTAT (Pebesma and Wesseling, 1998).

4. Results and discussion

4.1. Spatial structure of irrigation distribution

Fig. 5 shows the experimental indicator variogram calculated for the entire reconstructed irrigation map and the experimental variograms obtained when only the sampling locations of GPR and TDR are used instead of the entire map. Table 2 presents the variogram parameters fitted to these experimental variograms. These indicator variograms of irrigation distribution have no one-to-one relationship with SWC as the observed spatial redistribution of water by ponding during irrigation reduced the significance of the irrigation pattern. Nevertheless, the indicator variograms and the variogram model parameters in Table 2 show that: (1) the larger number of GPR sampling locations results in a smoother experimental variogram, (2) GPR and TDR variograms compare well, which means that the anisotropic sampling design of GPR did not distort the experimental variogram as would have been the case for an anisotropic irrigation distribution and (3) the expected range in SWC after irrigation is 10–15 m.

4.2. Spatial variation in soil water content

Fig. 6 presents the variograms of SWC measured with GPR and TDR before and after irrigation. The modeled variogram parameters are given in Table 2 along with the mean and total variance. The larger support of the GPR measurements has resulted in a lower variation in observed SWC, as can be seen from

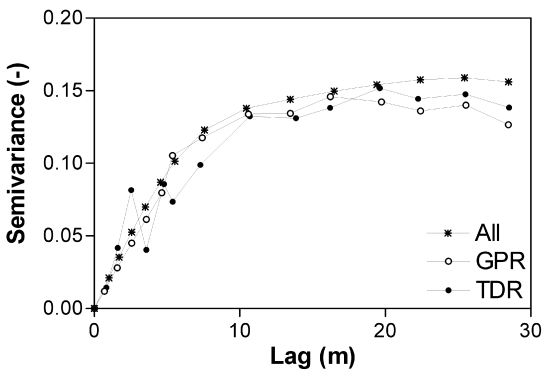

Fig. 5. Experimental indicator variograms of the heterogeneous irrigation distribution.

Table 2
Mean, variance, variogram parameters (range a, nugget c_0 and sill $c_0 + c$) and number of measurements (N) for soil water content ($m^3\ m^{-3}$) and indicator maps of irrigation

	Mean ($m^3\ m^{-3}$)	Variance $(m^3\ m^{-3})^2$	a (m)	c_0 $(m^3\ m^{-3})^2$	$c_0 + c$ $(m^3\ m^{-3})^2$	N
Irrigation (all)	0.446	0.2472	*12.8*	0	0.1535	4096
Irrigation (TDR)	0.485	0.2509	*13.8*	0	0.1430	216
Irrigation (GPR)	0.513	0.2500	*10.4*	0	0.1377	1416
TDR (before)	0.245	0.0017	*4.4*	0.0003	0.0012	213
TDR (after)	0.284	0.0024	*9.7*	0.0003	0.0017	215
GPR (before)	0.246	0.0007	*8.8*	0	0.0004	1383
GPR (after)	0.273	0.0010	*11.7*	0	0.0006	1416

Note that only range (in italics) of these variograms can be compared.

the comparison of the total variance and the sill variance. Some of the extra TDR variation is present in the nugget variance, which constitutes 24% of the sill variance before irrigation and 18% of the sill variance after irrigation. This nugget variance is caused by TDR measurement error and small-scale variation of SWC due to faunal activity, compaction by tractors, etc. Interestingly, the nugget variance of the GPR measurements was near zero, which indicates that: (1) most small-scale variation present in the TDR measurements is averaged out by the larger GPR measurement volume and (2) measurement error in GPR refractive index is low. Some caution is appropriate here because GPR semivariance estimates <5 m are measurements from the same transect (Fig. 3). This could lead to serially correlated measurement errors and apparently low nugget variances because transects are measured and

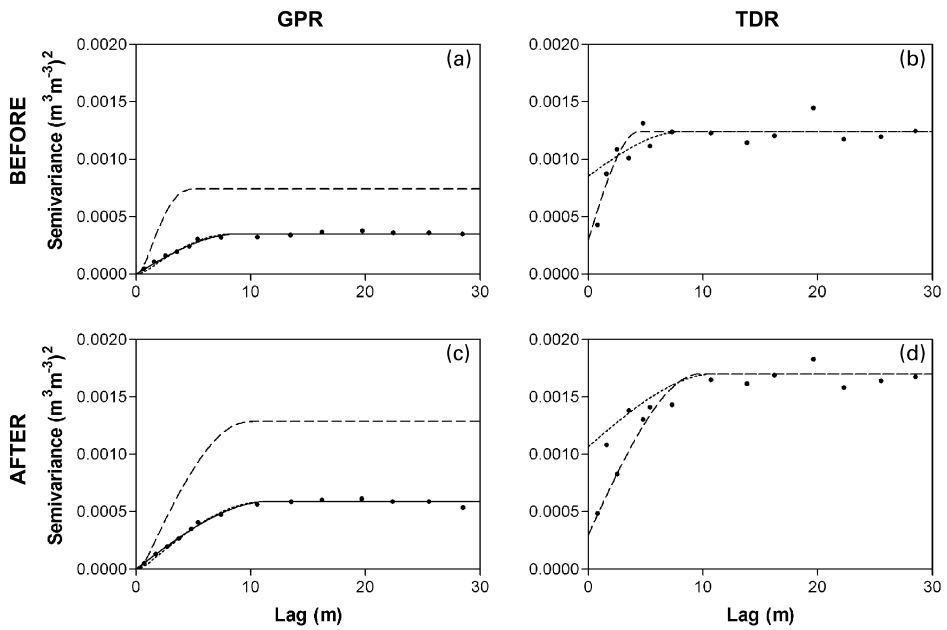

Fig. 6. SWC variograms measured with GPR (solid line in a and c) and TDR (dashed line in b and d) before and after irrigation. Dashed lines in a and c are the regularized TDR (block) variograms obtained after regularization of TDR variograms. Dotted lines are the inversely regularized TDR (point) variograms (b and d) obtained by computing the TDR variogram corresponding to GPR variogram after regularization. The quality of the fit is indicated by the dotted lines in a and c.

processed sequentially. However, the semivariance estimates >5 m seem to align nicely with the estimates <5 m, which suggests that serially correlated measurement errors are of minor importance. In future research the sampling scheme of GPR should include crossing transects to study the importance of correlated measurement errors on the short-range structure of the GPR variogram.

Table 2 and Fig. 6 show that the range of the SWC variograms increased from 4.4 to 9.7 m for TDR and from 8.8 to 11.7 m for GPR due to irrigation. This increase is caused by the large-scale structures in SWC created by irrigation (type A sprinklers). The range of the irrigation pattern was estimated as 10–15 m, which is closer to the range found for GPR than for TDR. However, the uncertainty in the TDR variogram range is high due to the noisy experimental TDR variogram and, therefore, the underestimation of the range by TDR is not necessarily significant. The GPR experimental variogram is much smoother and is based on more measurements and, therefore, the GPR model parameters are expected to be more reliable. This illustrates the key advantage of GPR over TDR. The non-invasive character of GPR allows the acquisition of a large number of measurements with a high sampling density, whereas the sampling density of TDR is limited by the need to install TDR sensors at each measurement locations.

Fig. 6 also shows the regularized TDR variograms (block support, dashed lines in Fig. 6a and c) obtained from the TDR variograms (point support, dashed lines in Fig.6b and d). It can be seen that regularization basically shifts the TDR variogram down by removing the nugget variance, which could be expected because the GPR measurement volume is several times smaller than the TDR variogram range. Ideally, the regularized TDR variogram should be identical to the GPR variogram because regularization compensates for the difference in support between the two methods. Clearly, this is not the case here. GPR measures less variation than expected from the regularized TDR variogram. To further study this discrepancy, we computed the TDR (point) variograms that result in the GPR variograms after regularization, hereafter referred to as the 'inversely regularized TDR variograms'. The dotted lines in Fig. 6b and d show the inversely regularized TDR variograms and the dotted lines in Fig. 6a and c illustrate the high quality of the fit. Similar to the regularization, the inverse regularization mainly shifts the GPR variogram up to the level of the TDR variogram. The purpose of this inverse regularization is to illustrate the sensitivity of the regularized TDR variogram to the choice of TDR nugget variance and range. The TDR-nugget variance was fixed to the independently determined value of 0.0003 $(m^3\,m^{-3})^2$, which is a slightly low value according to the fit in Fig. 6d, and, therefore, the discrepancy between the regularized and GPR variograms is especially large in Fig. 6c. A higher fitted nugget variance would have resulted in a smaller difference in Fig. 6a and c. However, the TDR nugget variance suggested by the inverse regularization seems too high. Therefore, it must be concluded that the difference in support between GPR and TDR cannot consistently be compensated with regularization, although the large differences in Fig. 6a and c are partly a reflection of the sensitivity of the regularization to the choice of the TDR nugget variance, which is an uncertain variogram model parameter.

A possible explanation for the failure of regularization is the depth of influence of the ground wave measurement, which theoretically decreases with increasing soil water content. Huisman et al. (2001) found no systematic difference between GPR measurements based on the ground wave and TDR measurements with a 0.10 m long probe. However, their results were based on SWC measurements for different soil types, presumably with relatively homogeneous SWC profiles with depth, and did not include a comparison with TDR probes with different lengths. For the soil in this study, there might have been a systematic difference between GPR and TDR measurement depths.

4.3. Soil water content mapping

Fig. 7 shows interpolated maps of SWC obtained from GPR and TDR measurements before irrigation. In general, both maps show similar results. For example, they both indicate that the initial SWC is rather high and that the wettest areas are in the SE part of the field. The mean difference between the maps of initial SWC is only 0.002 $m^3\,m^{-3}$ and the root mean square difference between the maps is 0.018 $m^3\,m^{-3}$ (see Table 3 for more statistics). Fig. 7 also illustrates

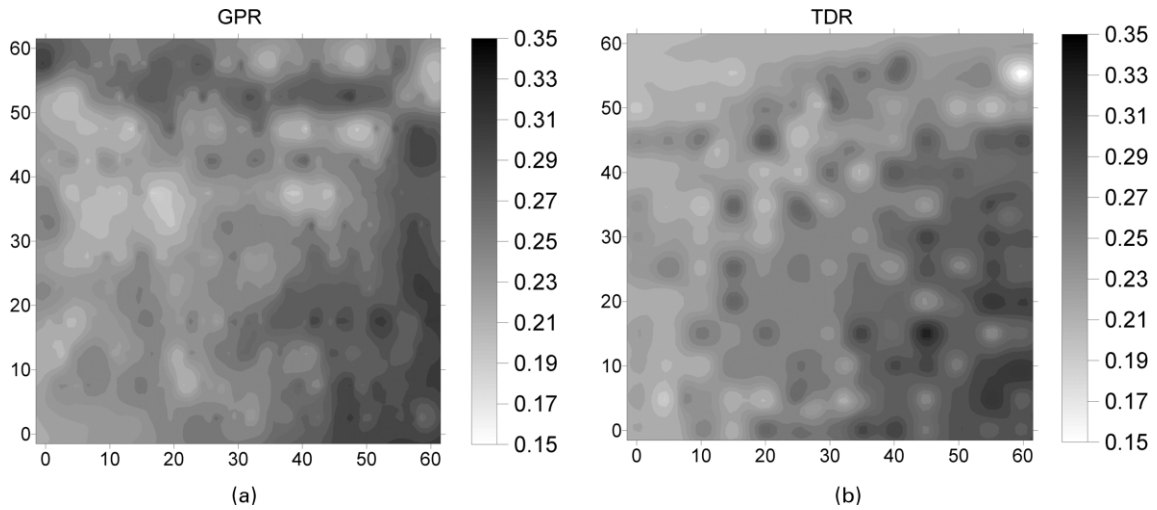

Fig. 7. Interpolated maps of initial soil water content ($m^3\ m^{-3}$) before irrigation, measured with GPR and TDR. Semivariograms used for interpolation with universal (block) kriging are presented in Table 2 and Fig. 6.

the influence of the sampling design and measurement support on the kriging predictions. Despite the use of block kriging, the interpolated map of TDR has a spotted appearance caused by the combined influence of the sample spacing and the short range for TDR. Fig. 8 shows the kriging variance corresponding to the interpolated maps of GPR and TDR shown in Fig. 7. Obviously, there is a strong dependence of the kriging variance on the sampling design (bands for GPR and dots for TDR). The root mean square kriging error was 0.011 $m^3\ m^{-3}$ for GPR and 0.025 $m^3\ m^{-3}$ for TDR. This difference in kriging variance is closely related to the discrepancy between the regularized TDR variogram and the GPR variogram discussed in Section 4.2.

Fig. 9 shows the increase in SWC due to irrigation as measured with GPR and TDR. These maps were obtained by subtracting interpolated maps of SWC measurements obtained after and before irrigation. Table 3 shows that the mean increase is 0.023 $m^3\ m^{-3}$ for GPR and 0.038 $m^3\ m^{-3}$ for TDR. This relatively large difference in mean increase is caused by the difference in mean SWC after irrigation, as the mean initial SWC was similar. This could indicate that strong contrasts in SWC profile with depth directly after irrigation have caused a systematic difference between GPR and TDR.

Comparison of Figs. 3 and 9 show that the large-scale structures in SWC (i.e. the two large sprinklers in the center) are clearly recognizable in case of both GPR and TDR. However, the boundaries between different SWC units are better resolved in the GPR map. In case of TDR, the boundary position can be determined down to 5 m, whereas GPR can determine the boundary position with a higher resolution of 0.5 m in the transect direction.

Small-scale structures in SWC (elements B, C and D in Fig. 3) are, in general, not well resolved by either the GPR or the TDR maps. This is partly due to high initial water content and the high sprinkling intensity of the small-scale structures, which caused ponding and lateral transport of water. However, close inspection of Fig. 9 shows that the increase in water content due to the small sprinkler D located at coordinates (40,55) is present in the GPR increase map because a measurement transect crosses this

Table 3
Comparison of interpolated maps of soil water content ($m^3\ m^{-3}$) before and after irrigation

	GPR	TDR	GPR–TDR		
	Mean	Mean	Mean	SD	RMSD
Before	0.247	0.245	0.002	0.018	0.018
After	0.270	0.283	−0.013	0.022	0.026
Increase	0.023	0.038	−0.015	0.023	0.027

SD is standard deviation and RMSD is the root mean square difference between GPR and TDR.

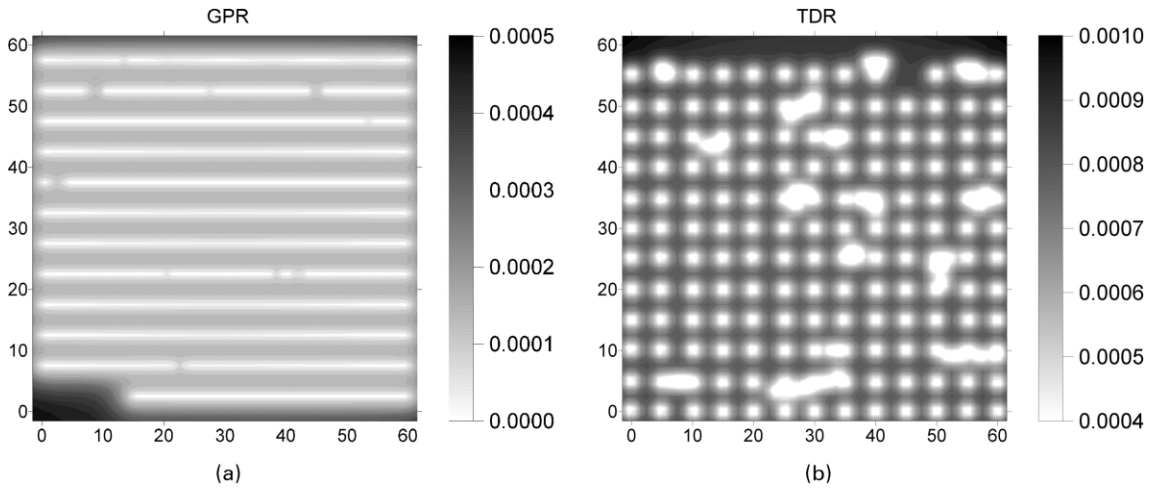

Fig. 8. Maps of kriging variance $(m^3\ m^{-3})^2$ corresponding to the interpolated maps of Fig. 7.

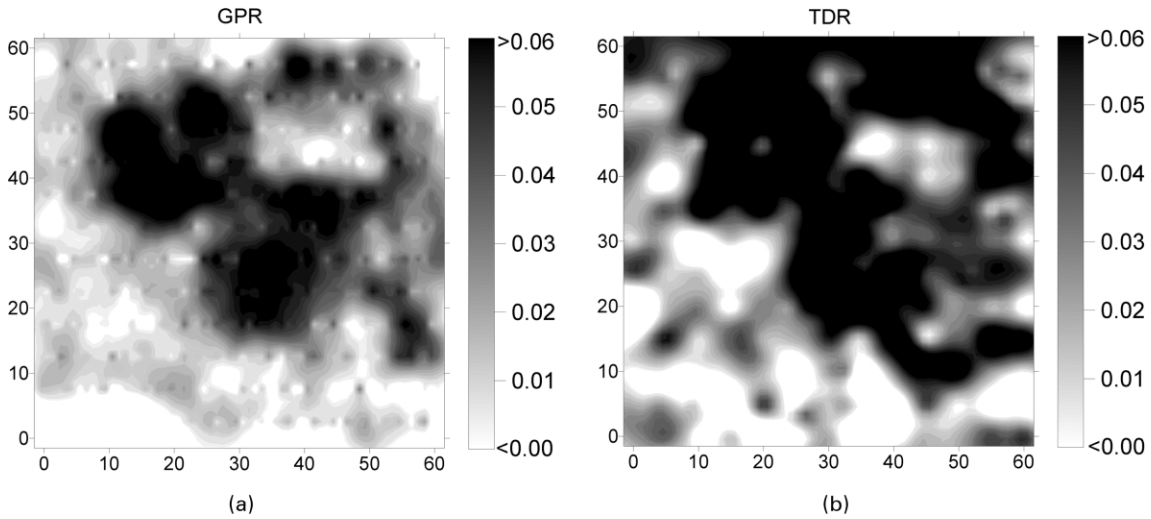

Fig. 9. Maps of increase in soil water content $(m^3\ m^{-3})$ due to irrigation. Maps were obtained by subtracting interpolated maps of soil water content before and after irrigation.

sprinkling location. For TDR, the line element running from (20,50) to (50,50) shows up in the increase map because the TDR grid was located beneath these sprinklers, whereas no GPR transect was located close to these sprinklers. These two examples illustrate the importance of the sampling strategy in determining whether small features are observed. Obviously, the detection of structures smaller than the sampling interval is based on chance. In this study, all structures smaller than 5 m are not necessarily resolved by either GPR or TDR, although the probability that small structures are detected by GPR is higher due to the small sampling interval in the x-direction (0.5 m).

5. Conclusions

The potential of GPR to map SWC at the field scale (3600 m^2) was evaluated with an experiment in which

a spatial structure in SWC was created by irrigation on a sandy loam soil. This small field size allowed a feasible comparison of GPR and TDR measurements. The comparison showed that GPR and TDR measured similar initial mean SWC. The measured SWC variation was lower for GPR due to the larger measurement volume. A comparison of the GPR and TDR variograms showed that the larger measurement volume of GPR resulted in a low nugget variance indicating that small-scale variation of SWC (<1.5 m) due to faunal activity, compaction by tractors, etc. often present in TDR measurements is averaged out in case of GPR. The large number of easily acquired GPR measurements also resulted in reliable experimental variograms and variogram model parameters. Generally, it was concluded that GPR is well suited to capture the spatial SWC variation as expressed by the variogram.

To extend the comparison between GPR and TDR variograms, the difference in measurement volume was compensated for by regularization. The regularized TDR variograms were largely different from the GPR variograms. This was partly attributed to the large sensitivity of the regularization to the choice of the TDR nugget variance, which is an uncertain model parameter due to relatively small number of TDR measurements at short separations. A further possible explanation for systematic differences between GPR and TDR is the unknown depth of influence of the ground wave measurement, which is an important GPR topic that needs to be resolved in future research.

GPR and TDR were also compared in terms of the kind of spatial structures that can be captured by each method. The comparison showed that GPR is better suited than TDR for mapping large-scale features in SWC. Especially the boundaries between areas with different SWC were better reproduced by GPR, among others because of the large number of measurements that can be acquired with GPR. Small-scale features were not mapped adequately by either GPR or TDR. However, the chance of detecting small features in SWC mapping at the field scale is higher for GPR, simply because of the higher sampling density. This is, of course, only true when the small-scale features are not distinctly smaller than the measurement volume of GPR.

In this particular study, the measurement effort was approximately equal for GPR and TDR because a small field of 60×60 m^2 was used. Generally, the acquisition time of GPR is determined by the speed of acquisition, which is limited by the ratio of the sampling interval (in m) and the trace acquisition time determined by sampling rate and the number of stacks per trace. There is a trade-off between acquisition time on the one side and data-quality and number of measurements on the other side. In case of our 60×60 m^2 field size, high-quality data were acquired with a high sampling density and this resulted in a low acquisition speed. However, in case of larger field sizes (see for example, Mohanty et al., 2000) high quality measurements can be acquired at much higher speed (up to $3-5$ km h^{-1}) because the required sampling density is often lower. Therefore, the ratio between the number of GPR and TDR measurements that can be acquired within the same time span increases dramatically in favor of GPR for larger fields. Thus, GPR is a much more attractive method for assessing the spatial variation of SWC of large fields or even catchments.

Acknowledgments

NWO-ALW grant numbers 750-19-804 and 809-32-003 financially supported this study. S.C. Dekker, M. van der Gulik, B. Jansen, K.J. Raat, M. van der Velde, A. Visser, P. de Willigen and especially L. de Lange are thanked for assistance during the fieldwork period. The constructive comments of one reviewer improved the quality of this paper.

References

Annan, A.P., 1973. Radio interferometry depth sounding. Part I. Theoretical discussion. Geophysics 38 (3), 557–580.

Bouten, W., Heimovaara, T.J., Tiktak, A., 1992. Spatial patterns of throughfall and soil water dynamics in a Douglas fir stand. Water Resources Research 28 (12), 3227–3233.

Brekhovskikh, L.M., 1960. Waves in Layered Media, Applied Mathematics and Mechanics, vol. 6. Academic Press, New York, 561 pp.

Chanzy, A., Tarussov, A., Judge, A., Bonn, F., 1996. Soil water content determination using a digital ground-penetrating

radar. Soil Science Society of America Journal 60, 1318–1326.
Davis, J.L., Annan, A.P., 1989. Ground-penetrating radar for high resolution mapping of soil and rock stratigraphy. Geophysical Prospecting 37, 531–551.
Du, S., 1996. Determination of water content in the subsurface with the ground wave of ground penetrating radar, PhD Thesis Ludwig-Maximilians-Universität, München, 117 pp.
Du, S., Rummel, P., 1994. Reconnaissance Studies of Moisture in the Subsurface with GPR, Fifth International Conference on Ground Penetrating Radar, Waterloo Centre for Groundwater Research, Waterloo, Kitchener, Ont., Canada, 1241–1248.
Famiglietti, J.S., Deveraux, J.A., Laymon, C.A., Tsegaye, T., Houser, P.R., Jackson, T.J., Graham, S.T., Rodell, M., van Oevelen, P.J., 1999. Ground-based investigation of soil moisture variability within remote sensing footprints during the Southern Great Plains 1997 (SGP97) hydrology experiment. Water Resources Research 35 (6), 1839–1851.
Ferré, P.A., Knight, J.H., Rudolph, D.L., Kachanoski, R.G., 1998. The sample areas of conventional and alternative time domain reflectometry probes. Water Resources Research 34 (11), 2971–2979.
Goovaerts, P., 1997. Geostatistics for Natural Resources Evaluation, Applied Geostatistics Series, Oxford University Press, Oxford, 483 pp.
Heimovaara, T.J., 1993. Design of triple-wire time domain reflectometry probes in practice and theory. Soil Science Society of America Journal 57, 1410–1417.
Heimovaara, T.J., Bouten, W., 1990. A computer-controlled 36-channel time domain reflectometry system for monitoring soil water contents. Water Resources Research 26 (10), 2311–2316.
Herkelrath, W.N., Hamburg, S.P., Murphy, F., 1991. Automatic, real-time monitoring of soil moisture in a remote field area with time domain reflectometry. Water Resources Research 27 (5), 857–864.
Heuvelink, G.B.M., 1998. Uncertainty analysis in environmental modelling under a change of spatial scale. Nutrient Cycling in Agroecosystems 50, 255–264.
Huisman, J.A., Sperl, C., Bouten, W., Verstraten, J.M., 2001. Soil water content measurements at different scales: accuracy of time domain reflectometry and ground-penetrating radar. Journal of Hydrology 245 (1–4), 48–58.
Hupet, F., Vanclooster, M., 2002. Intraseasonal dynamics of soil moisture variability within a small agricultural maize cropped field. Journal of Hydrology 261 (1–4), 86–101.
Jackson, T.J., Schmugge, J., Engman, E.T., 1996. Remote sensing applications to hydrology: soil moisture. Hydrological Sciences Journal 41 (4), 517–530.
Journel, A.G., Huijbregts, C.J., 1978. Mining Geostatistics, Academic Press, London, 600 pp.
Merz, B., Bardossy, A., 1998. Effects of spatial variability on the rainfall runoff process in a small loess catchment. Journal of Hydrology 212–213, 304–317.
Mohanty, B.P., Famiglietti, J.S., Skaggs, T.H., 2000. Evolution of soil moisture spatial structure in a mixed vegetation pixel during the Southern Great Plains (1997) (SGP 97) hydrology experiment. Water Resources Research 36 (12), 3675–3686.
Nissen, H.H., Moldrup, P., de Jonge, L.W., Jacobsen, O.H., 1999. Time domain reflectometry coil probe measurements of water content during fingered flow. Soil Science Society of America Journal 63, 493–500.
Paltineanu, I.C., Starr, J.L., 1997. Real-time soil water dynamics using multisensor capacitance probes: laboratory calibration. Soil Science Society of America Journal 61, 1576–1585.
Pebesma, E.J., Wesseling, C.G., 1998. GSTAT: a program for geostatistical modelling, prediction and simulation. Computers and Geosciences 24 (1), 17–31.
Ritsema, C.J., Dekker, L.W., 1998. Three-dimensional patterns of moisture, water repellency, bromide and pH in a sandy soil. Journal of Contaminant Hydrology 31 (3–4), 295–313.
Sperl, C., 1999. Erfassung der raum-zeitlichen Variation des Bodenwassergehaltes in einem Agrarökosystem mit dem Ground-Penetrating Radar, PhD Thesis Technische Universität München, München, 182 pp.
Topp, G.C., Davis, J.L., Annan, A.P., 1980. Electromagnetic determination of soil water content: measurements in coaxial transmission lines. Water Resources Research 16 (3), 574–582.
USDA, 1975. Soil Taxonomy: a Basic System of Soil Classification for Making and Interpreting Soil Surveys, Agric. Handbook 436, USDA (United States Department of Agriculture) Soil Conservation Service, Washington, DC.
van der Kruk, J., 2001. Three-dimensional imaging of multi-component ground-penetrating radar data, PhD Thesis Delft University of Technology, Delft, 242 pp.
van Overmeeren, R.A., Sariowan, S.V., Gehrels, J.C., 1997. Ground penetrating radar for determining volumetric soil water content; results of comparative measurements at two sites. Journal of Hydrology 197, 316–338.
Webster, R., Oliver, M.A., 2001. Geostatistics for Environmental Scientists, Wiley, Chichester.
Weiler, K.W., Steenhuis, T.S., Boll, J., Kung, K.-J.S., 1998. Comparison of ground penetrating radar and time domain reflectometry as soil water sensors. Soil Science Society of America Journal 62, 1237–1239.
Western, A.W., Blöschl, G., 1999. On the spatial scaling of soil moisture. Journal of Hydrology 217, 203–224.
Western, A.W., Blöschl, G., Grayson, R.B., 2001. Towards capturing hydrologically significant connectivity in spatial patterns. Water Resources Research 37 (1), 83–97.
Wood, E.F., 1997. Effects of soil moisture aggregation on surface evaporative fluxes. Journal of Hydrology 190, 397–412.
Yu, Z., 2000. Assessing the response of subgrid hydrologic processes to atmospheric forcing with a hydrologic model system. Global and Planetary Change 25, 1–17.